A Laboratory Model of Thermocline Depth and Exchange Fluxes across Circumpolar Fronts*

CLAUDIA CENEDESE

Physical Oceanography Department, Woods Hole Oceanographic Institution, Woods Hole, Massachusetts

JOHN MARSHALL

Department of Earth, Atmospheric and Planetary Sciences, Massachusetts Institute of Technology, Cambridge, Massachusetts

J. A. WHITEHEAD

Physical Oceanography Department, Woods Hole Oceanographic Institution, Woods Hole, Massachusetts

(Manuscript received 6 January 2003, in final form 7 July 2003)

ABSTRACT

A laboratory experiment has been constructed to investigate the possibility that the equilibrium depth of a circumpolar front is set by a balance between the rate at which potential energy is created by mechanical and buoyancy forcing and the rate at which it is released by eddies. In a rotating cylindrical tank, the combined action of mechanical and buoyancy forcing builds a stratification, creating a large-scale front. At equilibrium, the depth of penetration and strength of the current are then determined by the balance between eddy transport and sources and sinks associated with imposed patterns of Ekman pumping and buoyancy fluxes. It is found that the depth of penetration and transport of the front scale like $\sqrt{[(fw_e)/g']}L$ and w_eL^2, respectively, where w_e is the Ekman pumping, g' is the reduced gravity across the front, f is the Coriolis parameter, and L is the width scale of the front. Last, the implications of this study for understanding those processes that set the stratification and transport of the Antarctic Circumpolar Current (ACC) are discussed. If the laboratory results scale up to the ACC, they suggest a maximum thermocline depth of approximately $h = 2$ km, a zonal current velocity of 4.6 cm s^{-1}, and a transport $T = 150$ Sv (1 Sv $\equiv 10^6$ m^3 s^{-1}), not dissimilar to what is observed.

1. Introduction

In the Southern Ocean, meridional gradients in air–sea buoyancy flux act to create a strong polar front along which the Antarctic Circumpolar Current (ACC) flows in thermal wind balance. Westerly winds also drive the ACC eastward and, through associated Ekman currents, induce an Eulerian meridional circulation (the Deacon cell), which acts to overturn isopycnals enhancing the strong frontal region. The potential energy stored in the front is released through baroclinic instability, and the ensuing eddies are thought to play a fundamental role in the dynamical and thermodynamical balance of the ACC.

Figure 1a shows a highly idealized schematic diagram of a streamwise average view of the ACC. The ACC is imagined to flow along the frontal outcrop. Equatorward of the front, light fluid is pumped down from the surface through the action of the prevailing winds; polewards of the front heavy fluid is sucked up to the surface. Equatorward flow in the surface Ekman layer carries fluid meridionally at the surface balancing regions of upwelling and downwelling. However, what happens below the surface Ekman layer? How is the fluid returned poleward?

Here we set up and study an idealized laboratory model designed to address the possibility that eddy transfer may play an important role in this problem. The idea is sketched in Fig. 1b. Rather than suck and pump from the surface, we represent the action of the wind by pumping fluid in to and out of a rotating tank through many small holes drilled in its base. The fluid pumped in at the periphery of the tank from below is dense; (ambient) fluid pumped out in the center of the tank is less dense. The dense fluid pumped in from below represents, we imagine, the light fluid pumped down from the surface in the subtropics, as sketched in Fig. 1a.

As we shall see, in our laboratory experiment, the

* Woods Hole Oceanographic Institution Contribution Number 10887.

Corresponding author address: Dr. Claudia Cenedese, Physical Oceanography Department, Woods Hole Oceanographic Institution, MS #21, Woods Hole, MA 02543.
E-mail: ccenedese@whoi.edu

height of the dense fluid pumped in from the periphery increases, but the dense fluid is prevented from moving radially inward in an axisymmetric manner because of the Coriolis force due to the rotation of the tank. Instead it forms a circumpolar front that becomes baroclinically unstable and the radial transfer of fluid in to the central sucking region is achieved by unsteady, eddying motions (the horizontal wiggly arrows in Fig. 1b). Ultimately an equilibrium is set up in which (i) the radial volume transport by eddies balances the input of dense fluid and (ii) the height to which the dense fluid reaches is controlled by the efficiency at which eddies carry fluid radially.

Elsewhere (e.g., Marshall et al. 2002; Karsten et al. 2002; Marshall and Radko 2003) it has been argued that meridional eddy transfer, as described above, is the central mechanism that sets the depth and stratification of the ACC. Here we study this mechanism in a controlled laboratory setting. The external parameters of our system are the scale of the forcing region L, the volume flux pumped in to the tank Q, the buoyancy anomaly of the pumped fluid g', and the rotation rate of the tank Ω. Our goal is to understand how the height of the dense circumpolar front h and its velocity scale u depend on these external parameters.

Of particular interest is the manner in which this simple experiment combines both mechanical and buoyancy forcing of the fluid. Previous laboratory studies have concentrated on either mechanical or buoyancy forcing but seldom in combination. Laboratory studies of the wind-driven circulation started with the ''sliced cylinder'' model introduced by Pedlosky and Greenspan (1967) and Beardsley (1969). These studies have been followed up by further experimental, analytical, and numerical studies (Beardsley 1973, 1975; Beardsley and Robbins 1975; Becker and Page 1990; Griffiths and Veronis 1997, 1998). Although these models apply to gyre circulation, they are not directly relevant to circumpolar flow because here Sverdrup dynamics do not apply. Narimousa and Maxworthy (1985, 1987) studied a two-layer stratified model of coastal upwelling. Some aspects of that model—the horizontal density gradient and the wind stress forcing—have processes in common with the ACC front. However, the presence of a coastline and a prescribed stratification prohibit its direct application to the problem at hand. Some laboratory studies of baroclinic zonal currents are reviewed by Rhines (1994) including the dynamics and transport of Rossby waves and currents explored by, for example, Sommeria et al. (1989, 1991).

The instability of a buoyancy-driven current in the absence of wind stress has been comprehensively discussed by Eady (1949), Phillips (1954), Hide (1971), Hart (1972, 1980), Douglas et al. (1972), Saunders (1973), Griffiths and Linden (1981a,b, 1982), Chia et al. (1982), Condie and Rhines (1994) and many others. The Rossby radius of deformation, normalized by the horizontal lengthscale of the flow, is the controlling factor—when this parameter is less than $\sim$ unity, baroclinic waves with subsequent eddy formation appear at the density front. Again, these models capture some aspects of the ACC, but only recently have laboratory models that combine both buoyancy and wind-driven components been developed—see Marshall et al. (2002) who studied a warmed, pumped lens on an ''f'' plane. Furthermore, Ivey et al. (1995) and Rosman et al. (1999) preconditioned a convective region with cyclonic or anticyclonic circulation using both buoyancy and mechanical forcing. They then investigated the effects of preconditioning on the lateral spreading of deep water formed during open ocean convection. Here we present a laboratory experiment designed to address the combined mechanical and buoyancy forcing of an initially unstratified rotating flow in a geometry relevant to circumpolar flow.

Our paper is set out as follows. In section 2 we describe the apparatus used in the experiment and the measurements taken. In section 3 we describe the phenomena and evolution of typical circumpolar flows obtained. We formulate a theory in section 4 and apply it to interpret our results. The possible implications of this study to our understanding of oceanic circumpolar flows are described in section 5.

2. Experimental setup

As discussed in the introduction, instead of pumping light fluid down from above as in Fig. 1a, in our laboratory abstraction we flip things in the vertical and gently pump (i.e., small flow rate) dense fluid ρ_1 up from below around the periphery of a rotating tank (representing light water being pumped down in the subtropics) and gently withdraw lighter fluid of density ρ_2 at the center (representing the pole) as shown on Fig. 1b.

The experiments were conducted in a glass tank of radius $R = 50$ cm, filled with fluid of density ρ_2 to a depth $H = 30$ cm, and mounted on a direct-drive turntable rotating counterclockwise. A sketch of the apparatus is shown in Fig. 2. We simulate the action of Ekman layers on the interior fluid by introducing and withdrawing fluid through a perforated base at a controlled rate. By adjusting the rate of pumping and the density of the pumped fluid, we can independently control both the rate of the simulated Ekman pumping and the magnitude of the buoyancy flux. Underneath the perforated false bottom, there is a reservoir divided into an inner region of radius R_1, an intermediate annular region of width $(R_2 - R_1)$, and an outer annular region of width $(R - R_2)$ (see Fig. 2b). Dense water, created by salt solution of density ρ_1, is fed into the outer annular region by means of a pump positioned in a dense water (ρ_1) source. This mechanical source simulates the vertical Ekman pumping, w_e, due to winds at the free surface of the ACC. The radius R_2 is the model's ''zero-wind-stress curl line'' and marks the position of the major frontal region that develops. The dense fluid is

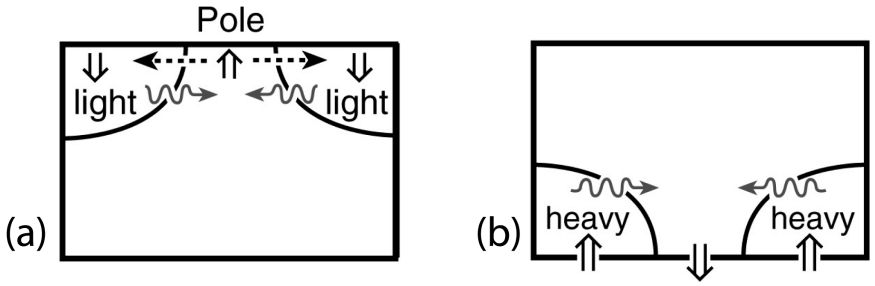

FIG. 1. (a) Sketch of a streamwise average view of the Antarctic Circumpolar Current. The dashed arrows indicate the meridional flow in the surface Ekman layer. The likely role of eddies in the cross-stream transfer of fluid below, represented by the wavy arrows, is studied in this paper. (b) Sketch of the flow in an idealized laboratory model. If we flip (b) over in the vertical we obtain something resembling the sketch (a).

pumped into the tank with a flow rate Q through an area $A_e = \pi(R^2 - R_2^2)$, with an average vertical velocity $w_e = QA_e^{-1}$. The velocity at each hole is equal to $w_{\text{hole}} = Q(NA_{\text{hole}})^{-1}$ where $A_{\text{hole}} = \pi(d/2)^2$, N is the number of holes in the outer circular annulus, and d is the diameter of each hole. We choose $N = 1000$ and $d = 0.65$ cm such that w_{hole} is small enough to ensure that no ''jetting'' is observed upon introduction of the dense fluid for the range of flow rates covered. The fluid withdrawn from the inner region of radius R_1 is regulated by a pump with a flow rate Q_w. At the pumping rates employed, the flushing time of the apparatus is several hours.

A video camera mounted above the tank and coro-

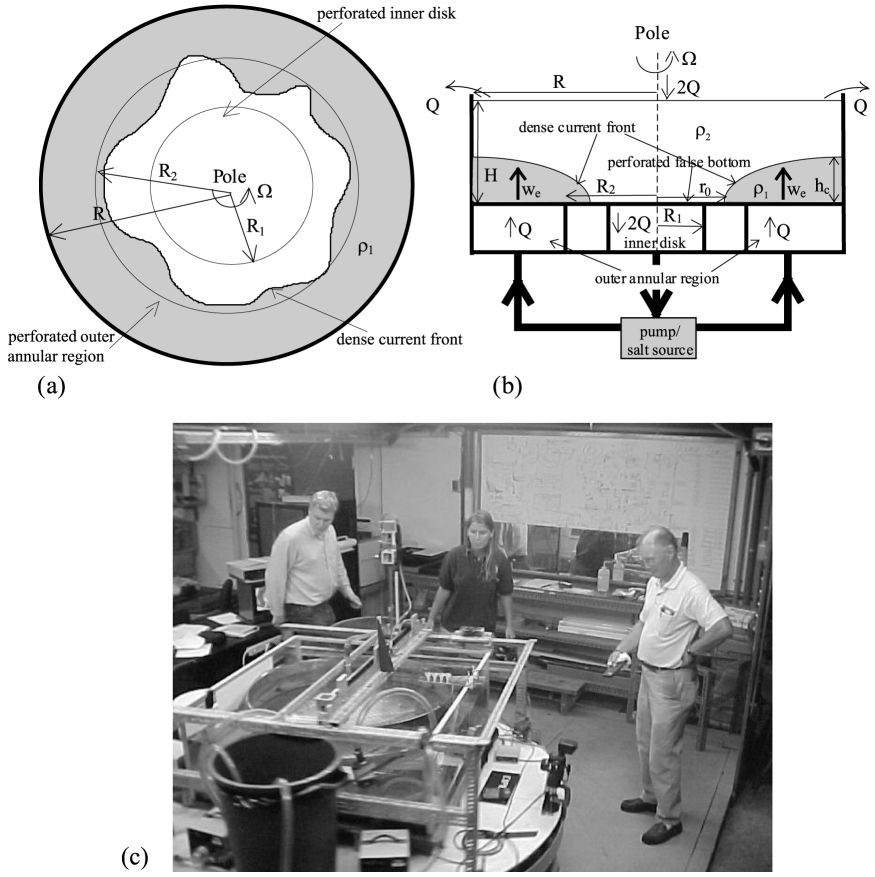

FIG. 2. The experimental apparatus: (a) top view and (b) side view. The arrow in the cyclonic direction in (a) and (b) indicates the counterclockwise direction of rotation of the tank. (c) The authors with the laboratory apparatus in the Geophysical Fluid Dynamics Laboratory at Woods Hole Oceanographic Institution, summer 2001.

TABLE 1. Overview of the experimental parameters (columns 2–4) and measured quantities (5–6).

Expt No.	f (s^{-1})	g' (cm s^{-2})	w_e (cm s^{-1})	h_e (cm)	u_e (cm s^{-1})
11	2	1.77	4.16×10^{-3}	4.9	0.33
12	3	2.06	4.16×10^{-3}	7.0	0.23
13	1	2.16	4.16×10^{-3}	6.8	0.74
14	2	0.39	4.16×10^{-3}	11.4	0.13
15	2	8.34	4.16×10^{-3}	6.1	0.84
16	1	0.29	4.16×10^{-3}	7.6	0.14
18	3	7.95	4.16×10^{-3}	6.4	0.50
19	3	0.49	4.16×10^{-3}	16.2	0.09
21	3	0.39	8.32×10^{-3}	21.9	0.23
22	3	0.39	2.08×10^{-3}	8.9	0.16
23	2	0.39	2.08×10^{-3}	5.9	0.13
24	3	1.96	8.32×10^{-3}	11.3	0.60
25	3	1.77	2.08×10^{-3}	7.9	0.14
26	2	0.39	8.32×10^{-3}	23.2	0.33
27	3	0.39	1.04×10^{-3}	15.2	0.09
28	3	1.86	1.04×10^{-3}	6.5	0.20

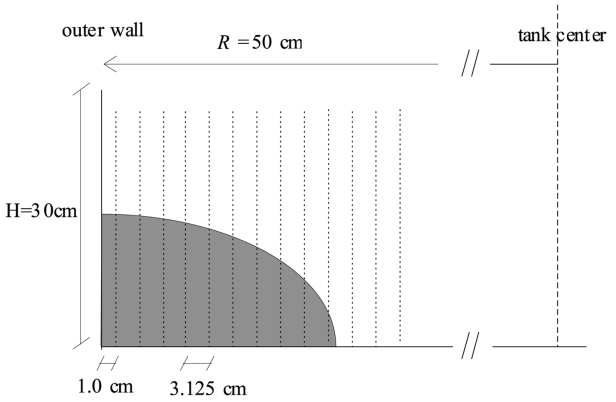

FIG. 3. The dotted lines indicate the position, along the radial section, where the density profiles were obtained using the conductivity measurements. The profiling section started 1 cm from the outer wall and the vertical profiles were positioned at an equal distance of 3.125 cm between each other until they reached a radius $r = 11.5$ cm.

tating with the tank, allows us to track and record on tape the circulation in the tank made visible with dye. The motion of the dense (dyed) current was observed both from the top and side of the tank to yield a three-dimensional view of the flow.

The dense fluid was continuously pumped into the bottom reservoir of the outer annular region until it filled up, when it entered the tank through the perforated bottom in the outer circular annulus, with very little observed mixing. The fluid was continuously supplied and formed a dense current with a height that increased in time.

In our experiments, the width of the dense current that develops was approximately equal to that of the outer annular region, $L = (R - R_2)$ (see Fig. 2). In order to obtain a baroclinically unstable current (Griffiths and Linden 1981b; Cenedese and Linden 2002), L was chosen to be several times larger than the expected Rossby radius of deformation of the current $R_c = (g'h_e)^{1/2}/f$, based on the predicted current height at equilibrium h_e (see section 4), the reduced gravity $g' = g(\rho_1 - \rho_2)/\rho_2$ and the Coriolis parameter $f = 2\Omega$, where Ω is the rotation rate of the tank. We found that $(R - R_2)/R \sim 1/3$ worked well with $R_2 = 35$ cm. The flow rate Q was varied between 0.42 and 33.33 $cm^3\ s^{-1}$, the Coriolis parameter f assumed values of 1, 2, and 3 s^{-1}, and the reduced gravity g' was varied between 0.3 and 8.0 $cm^2\ s^{-1}$ as shown in Table 1.

A conductivity probe was used to obtain the density structure along a radial section. This section started 1 cm from the outer wall and the probe traversed a vertical profile over the depth of the tank every 3.125 cm until it reached a radius $r = 11.5$ cm (see Fig. 3) after crossing the density front. The vertical spacing of the conductivity measurements was 0.1 cm. The time employed to complete one radial section was just over 60 s, which is less than the eddy evolution time scale. From these radial density sections we were able to determine the position of the density interface and hence the height of the dense current during the experiment. Furthermore, a measure of the vertical shear of the horizontal circumpolar current was obtained by dropping potassium permanganate crystals along a radial section across the dense current. Digital pictures of the purple streak left behind by the crystals were taken in a plane orthogonal to the radial section at fixed time intervals. The sequence of pictures gave a measure of the relative velocities in the two layers as shown in Fig. 4.

Preliminary test experiments

Initially a number of purely mechanically driven experiments were performed in which fluid having the same density as the environmental fluid (ρ_2) was pumped into the tank through the outer annular region with a vertical velocity w_e, and fluid was withdrawn from the middle of the tank at a rate $Q_w = Q$. Figure 5(I)a illustrates schematically the flow established during these experiments. A cyclonic barotropic zonal current developed, as expected from angular momentum considerations. The current was observed by dropping potassium permanganate crystals along a radial section. The maximum zonal velocity occurred at $r = R_2$, the radius at which the bottom vertical pumping vanished.

If, now, the water pumped in at the periphery is dense (ρ_1) and environmental fluid (ρ_2) is extracted at the center at a rate $Q_w = Q$, then a bottom-intensified cyclonic circulation is induced. This can be seen as follows. A dense ring of fluid (ρ_1) induces the thermal wind flow field shown in Fig. 5(I)b, anticyclonic above, cyclonic below. Thus the combined action of mechanical pumping and buoyancy forcing induces a flow that is a combination of the two induced flows shown in Figs. 5(I)a and 5(I)b. The result shown in Fig. 5(I)c is a strong, bottom-intensified cyclonic current with a weaker circulation above. The direction of this circulation above

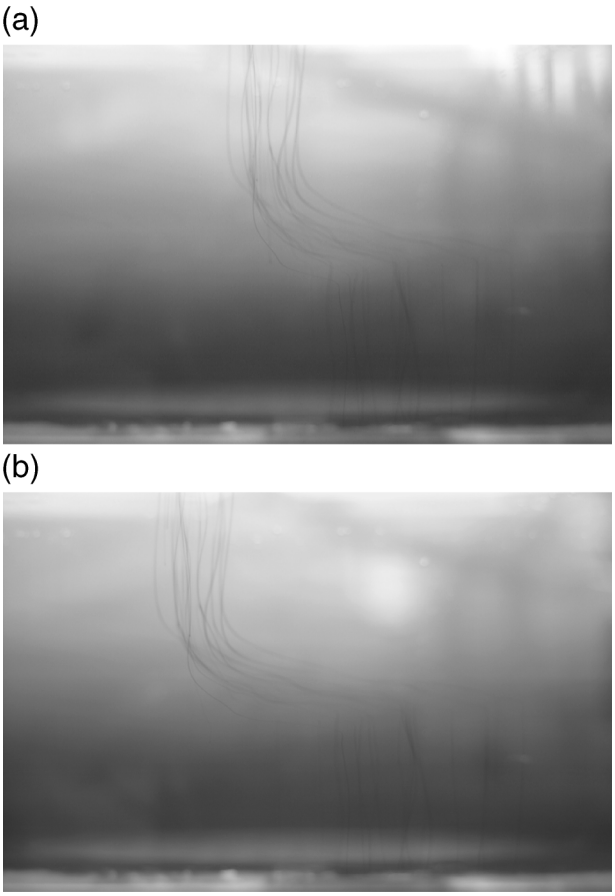

FIG. 4. Potassium permanganate streaks left behind the sinking crystals at two time intervals separated by 4 s. The upper light fluid is moving from right to left and the bottom blue dense fluid is slowly moving from left to right. The bottom Ekman layer flow is orthogonal to this field of view, and therefore it is not visible here.

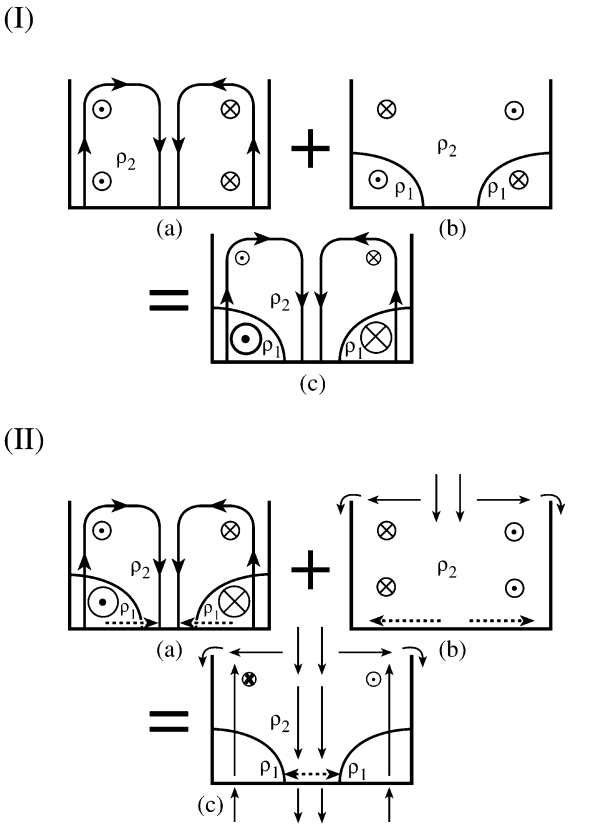

FIG. 5. Sketch illustrating (I) (a) mechanical forcing, (b) buoyancy forcing, and (c) a combination of the two in which the dense fluid (ρ_1) is pumped in the outer annular region and environmental fluid (ρ_2) is withdrawn through the center of the tank. (II) (a) Same as I(c); (b) fluid of density ρ_2 is pumped at the free surface with fluid overflowing the outer wall; (c) the resulting flow circulation when both (a) and (b) are applied. The dashed arrows in (a), (b), and (c) indicate the fluid motion in the laboratory bottom Ekman layers.

the dense fluid is given by the relative magnitude of the cyclonic [Fig. 5(I)a] and anticyclonic [Fig. 5(I)b] circulation in the top part of the tank. In the experiments described in this paper, the circulation above the dense fluid was always cyclonic, as shown in Fig. 5(I)c. Furthermore, the presence of the bottom cyclonic current, with its maximum velocity at $r = R_2$, is clearly seen in experiments in which dense fluid was pumped upward and ambient fluid removed from the center at the same rate.

We immediately note a problem, however: the presence of the bottom cyclonic current induces an Ekman flow directed radially inward, toward the sucking region. When the experiment is carried out with $Q_w = Q$ we observe that the dense fluid pumped upward around the periphery is removed via inward radial flow in the bottom Ekman layer to the sink region over the center of the tank, as sketched by the dashed arrows in Fig. 5(II)a. In these experiments the height of the dense current increases very slowly and the front is never observed to meander or become unstable. Such a radial Ekman inflow has no counterpart in the oceanographic system that we are attempting to model. As can be seen in Fig. 1a, the sense of the Ekman flow at the sea surface is to enhance the front rather then to dissipate it.

Therefore, in order to obtain a bottom Ekman layer moving radially outward, from the center of the tank to the outer wall, we ''added'' a suitable barotropic component to the flow by pumping in light fluid of the same density ρ_2 as the environment. This fluid was pumped in at the free surface at $r = 0$ cm as shown in Fig. 5(II)b, and a rate Q_{ρ_2}. This flow rate was chosen to be $Q_{\rho_2} = 2Q$ of which an amount $Q_o = Q$ overflows over the outer wall of the tank since the dense fluid is pumped into the tank with a flow rate Q while environmental fluid is extracted at the center at a rate $Q_w = 2Q$. The overflow rate Q_o was distributed along a large circumference (314 cm) and did not disturb the motion of the dense current in the lower part of the tank. However, the introduction of fluid at the free surface in the middle of the tank is efficient in generating a barotropic anticyclone, as shown in Fig. 5(II)b. This anticyclone is

sufficient to reverse the direction of the bottom Ekman layers, driving fluid from the center outward, as indicated by the dashed arrows in Fig. 5(II)c.

In summary, in the final configuration of the experiment we simultaneously pumped fluid of density ρ_2 at the free surface, pumped dense fluid (ρ_1) in the outer annular region, and withdrew environmental fluid (ρ_2) through the center of the tank while allowing fluid to overflow over the outer wall circumference [see Fig. 5(II)c]. The resulting circulation resembles that sketched in Fig. 1a, as required. Provided that the interface of the upwelling dense fluid around the periphery remains sufficiently far from the free surface, the radial outflow at the upper surface should have little influence on the behavior and motion of the dense bottom current. Similarly, we hypothesize that, in the ocean, the bottom Ekman layer has a negligible influence on the behavior of the surface front. In the presence of this anticyclonic barotropic background flow, we choose our system of reference to corotate with this background flow. This choice has been made to simplify the theoretical model in section 4 that does not consider the barotropic component of the flow induced by the flux of light fluid at the free surface. In this configuration, the bottom of the tank rotates cyclonically with respect to the background flow. Hence, the flow in the bottom Ekman layer is outward, as required.

If the Ekman flow is directed radially outward, then the only way in which the dense fluid pumped into the outer annular region can be carried radially inward is by flow in the interior of the dense fluid above the Ekman layer. We will see that this radial transfer is achieved by unsteady, eddying flow provided $R_c \ll (R - R_2)$.

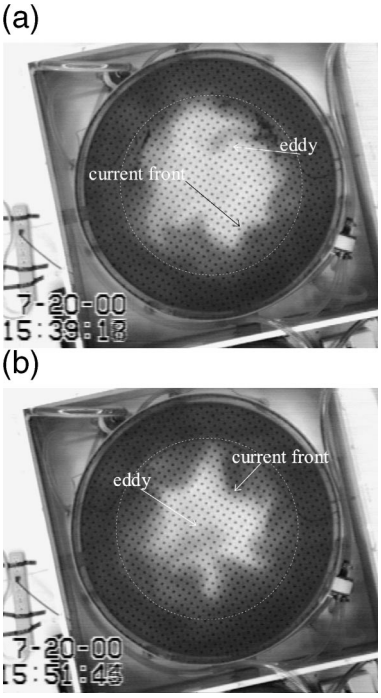

FIG. 6. Results from a typical laboratory experiment. The dense fluid pumped in from below is dyed and the grayscale is an indication of the height of the dense layer: (a) after 1060 rotation periods and (b) after 1145 rotation periods. The white dotted line indicates the inner limit of the outer circular annulus. ($f = 3\ s^{-1}$, $g' = 2\ cm\ s^{-2}$, $w_e = 3.910^{-3}\ cm\ s^{-1}$, $H = 20$ cm). The dots are the holes that make up the perforated base of the tank.

3. Typical evolution of eddying circumpolar flow

We carried out an extensive set of experiments with the combination of forcing mechanisms illustrated in Fig. 5(II)c, as set out in Table 1. During these experiments the dense dyed fluid was gently and continuously pumped in through the base building up a layer of dense fluid around the outer annular region. From the side glass wall it was possible to observe that the dense current had its maximum height at the outer wall. The height of the dense current gradually decreased along a radial section. Furthermore, potassium permanganate crystals were dropped into the tank to observe the direction of the flow in the bottom Ekman layer. The source/sink arrangement [Fig. 5(II)c] ensured the fluid was always observed to move radially outward in the bottom Ekman layer of the intermediate annular region of width ($R_2 - R_1$), outside of the dense current, due to the background barotropic anticyclonic motion generated by pumping fluid at the free surface (see section 2). Within the dense current, fluid in the bottom Ekman layer was directed either radially inward or outward depending on the magnitude of the baroclinic part of the flow associated with the dense current, relative to the background barotropic anticyclonic motion. When the baroclinic flow magnitude was larger (smaller) than the barotropic flow, the bottom Ekman layer within the dense current was directed radially inward (outward). In the system of reference used (i.e., as if we were moving within the anticyclonic background flow, see section 2) the dense current was always observed to circulate cyclonically.

After the dense current reached a critical height, the circumpolar front started meandering, with a growing wave-like disturbance at the interfacial front. The predominant wavelength of these disturbances scales with, and is a few times larger than, the Rossby radius of deformation of the dense current. Disturbances of the dyed dense fluid along the front were everywhere anticyclonic, and after an initial stage the non-axisymmetric disturbances grew and generated anticyclonic eddies that detached from the dense current and moved toward the center of the tank as shown in Fig. 6. In between those dense anticyclonic eddies, cyclonic eddies of clear ambient fluid were also observed. After reaching the center of the tank, the fluid in the dense eddies was withdrawn by suction, allowing more eddies to form and move to the center of the tank. Once the eddies appeared, the topography of the interface be-

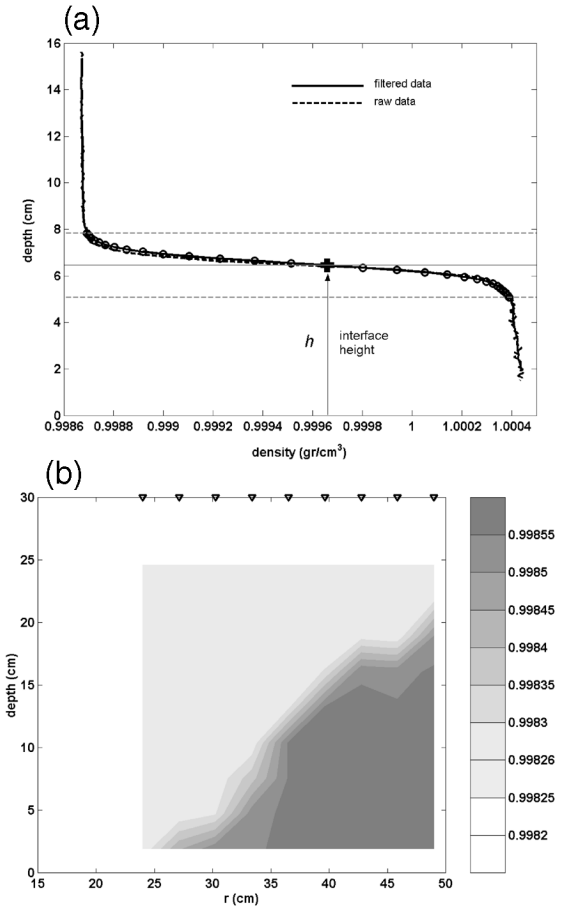

FIG. 7. (a) Vertical density profile showing the dense current below and the fresh layer above. The dashed gray lines indicate the thickness of the interface and the solid gray line the interface height. (b) Typical radial density section in which the dense fluid is shown in darker gray and the finite thickness of the interface is visible. The triangles at the top indicate the position of the density profile.

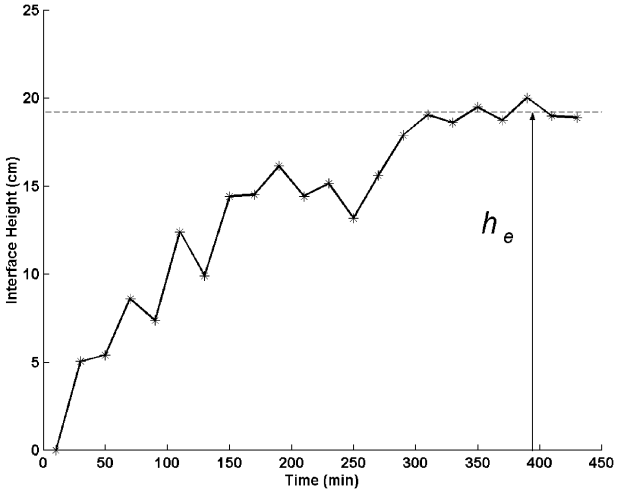

FIG. 8. The height of the interface near the outer wall plotted as a function of time. The interface upwelled until it reached a critical value that remained constant thereafter, indicating an equilibrium between lateral eddy volume flux and upward flux of dense fluid from below.

tween the dense and light fluid changed in character. The maximum height of the interface was still found at the outer wall, but it no longer decreased monotonically along a radial section. The density interface was clearly marked by the eddies having the classical convex shape where the interfacial height of the dense current was observed to increase and then decrease (after passing the center of the eddy) along a radial section. Furthermore, potassium permanganate crystals were used to observe the circulation within the eddies. The dense eddies all had a vigorous anticyclonic circulation that slowly weakened as the eddies left the dense current and moved radially inward toward the tank's center.

Density profiles obtained during the experiments (see section 2) charted the evolving stratification and the establishment of a two-layer system with an interface thickness of only a few centimeters. A typical density profile is shown in Fig. 7a where the dashed black line represents the raw data and the solid black line the values of the data after applying a boxfilter with a window size of 0.8 cm. The thickness of the interface between the fluids of density ρ_1 and ρ_2 is indicated in Fig. 7a by the open circles. The height of the interface above the bottom was chosen to be the middle point of the defined interface and is represented in Fig. 7a by the solid cross. The values of the interface height above the bottom were determined along a radial section (Fig. 3) at different times during the experiments. A typical radial section for a given time is shown in Fig. 7b. The triangles at the top indicate the radial position of the measurements. The dense current attained its maximum height at the outer wall $r = R = 50$ cm. The height of the interface between the dense current and the ambient fluid decreased inwards toward the center of the tank ($r \to 0$), as observed by eye from the side wall of the tank. To estimate the height of the dense current at the wall we chose to average the values of the interface height of the three profiles closest to the outer wall ($R = 50$ cm). This height increased over the course of the experiment as shown in Fig. 8. It then attained an equilibrium value, which we call h_e, that remained relatively constant in time. Hence, we infer that, in this equilibrium state, the lateral transport of fluid away from the current by eddies balances the mass inflow of dense water from below.

In addition to this equilibrium height we measured the vertical shear of the current making use of the vertical dye streaks recorded by the digital camera, as shown in Fig. 4.

4. Theoretical model

As suggested by the vertical density profiles presented in Fig. 7, we model the system using a 1½-layer shallow

water model with a mass source representing the inward pumping of fluid and a mass sink to represent eddy shedding. The interior flow is assumed to be in geostrophic and hydrostatic balance with a constant Coriolis parameter $f = 2\Omega$. The relevant nondimensional parameters will be discussed in section 5a when we compare the results of this study with observations.

We assume the Ekman number to be small and that the interior flow is in geostrophic balance. The steady-state governing equations, for which the Ekman layers are balanced, are

$$f\mathbf{k} \times \mathbf{u} = g'\nabla h, \quad \text{and} \tag{1}$$

$$\nabla_h \cdot (\mathbf{u}h) + w_e + w^* = 0, \tag{2}$$

where h is the mean height of the density interface, $\mathbf{u}$ is the mean horizontal velocity, $\mathbf{k}$ is a unit vector in the vertical direction, w_e is the imposed Ekman pumping, and

$$w^* = \nabla_h \cdot (\overline{\mathbf{u}'h'}) \tag{3}$$

is the vertical velocity associated with divergence of the cross-front volume flux. We assume that this ''bolus'' flux is dominated by the contribution from geostrophic eddies as they transport volume from the periphery to the center of the tank.

At equilibrium, we must have, integrating over the forcing volume given by the outer annular region of width $(R - R_2)$,

$$Q + \widetilde{w^*} = 0, \tag{4}$$

where Q is the integral of the pumping into the forcing volume through the base of the tank and $\sim$ is an integral over this region. Assuming azimuthal symmetry and approximating $\widetilde{w^*}$ by $2\pi[(R + R_2)/2]\overline{v'h'}$, where $\overline{v'h'}$ is the radial bolus flux (assumed positive if directed inward) and $2\pi(R + R_2)/2$ is the perimeter through which the flux occurs, we find that

$$\overline{v'h'} = \frac{Q}{2\pi\dfrac{R + R_2}{2}}. \tag{5}$$

If we now assume that the eddies transfer properties down the large-scale gradient, we can express the lateral eddy volume flux in terms of mean flow quantities as

$$\overline{v'h'} = -K\nabla\overline{h} = cu_e h_e, \tag{6}$$

where[1] $K = cLu_e$ is the eddy diffusivity, L is a transfer scale (see section 6 for details on the length scale used), c is an eddy efficiency parameter, and $\nabla\overline{h}$ has been replaced by $-(h_e/L)$. Here we assume that $L = R - R_2$ is the width of the forcing region and h_e is the maximum height of the density interface at equilibrium. The equilibrium thermal wind velocity scale u_e of the azimuthal flow is given by

$$u_e = \frac{g'h_e}{fL}, \tag{7}$$

using Eq. (1).

Combining Eqs. (5), (6), and (7), we find[2] that $h_e = \sqrt{1/c}\sqrt{fQL/[\pi(R + R_2)g']}$ or, substituting $Q = w_e\pi(R^2 - R_2^2)$ and $L = R - R_2$,

$$h_e = \sqrt{\frac{1}{c}}\sqrt{\frac{fw_e}{g'}}L. \tag{8}$$

The associated velocity scale is, using Eq. (7),

$$u_e = \sqrt{\frac{1}{c}}\sqrt{\frac{w_e g'}{f}}. \tag{9}$$

The transport T across a radial section of height h_e and width L can be expressed as

$$T = u_e h_e L = \left(\sqrt{\frac{1}{c}}\sqrt{\frac{w_e g'}{f}}\right)\left(\sqrt{\frac{1}{c}}\sqrt{\frac{w_e f}{g'}}L\right)L = \frac{1}{c}w_e L^2 \tag{10}$$

and depends only on the horizontal scale L, the eddy efficiency parameter c and the mechanical forcing w_e. It is important to note that Eq. (10) is an overestimate of the circumpolar current transport across a radial section since the radial section is not square; on the other hand one-half of Eq. (10) would be an underestimate since the radial section is not triangular either (see Fig. 7b). We will see below that the measured transport is roughly 70% of that given by Eq. (10).

Interpretation of experimental results in terms of the theory

Both the equilibrium height h_e, measured using the three profiles closest to the wall (see section 3), and the equilibrium mean horizontal velocity u_e, obtained making use of images such as Fig. 4, enabled us to estimate a value for the eddy efficiency parameter c as follows. At equilibrium Eq. (5) holds and so, using Eq. (6),

$$c = \frac{Q}{h_e u_e 2\pi\left(\dfrac{R + R_2}{2}\right)}. \tag{11}$$

The values of the eddy efficiency parameter obtained using Eq. (11) range between 0.01 and 0.06 with a mean

[1] See Jones and Marshall (1997) and Marshall et al. (2002) where the arguments in support of Eq. (6) are summarized.

[2] If we express Eq. (8) in terms of the vertical buoyancy flux, $B = w_e g'$, then we find

$$h \sim \sqrt{\frac{f}{B}}w_e L,$$

which is the scaling of the depth of the warmed, pumped ''f plane'' lens found in Marshall et al. (2002) and studied in Radko and Marshall (2003).

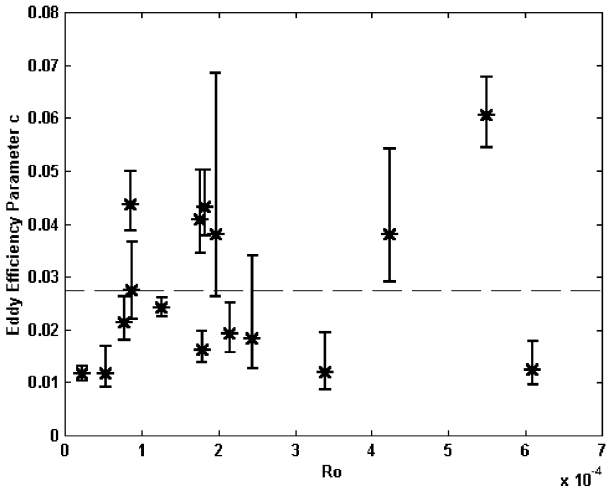

FIG. 9. Values of the eddy efficiency parameter c, evaluated assuming the balance Eq. (11), vs the Rossby number Ro $= w_e/h_e f$ that compares the rotation time scale with the vertical advective time scale (discussed fully in section 5a). The dashed line represents the mean value of $c = 0.027$.

value equal to 0.027, as shown in Fig. 9.[3] The scatter of the data points in Fig. 9 is possibly due to the fact that we are dealing with turbulent flows and we can only take measurements for a small sampling time after equilibrium is reached. The measurement technique described in section 2 cannot be automated and further lengthening the duration of the experiments (i.e., to last more than approximately 10 h) would have been beyond our capabilities. The vertical bars in Fig. 9 represent the values that c would have if, instead of choosing a point on the density interface (cross on Fig. 7a), we choose the whole interface thickness (open circles on Fig. 7a). We could not find evidence of a dependence of c on any of the external variables f, g', w_e or the nondimensional parameters, Bu and Ro, introduced in section 5a (Fig. 9).

From Eqs. (8) and (9) and the evaluated value of $c = 0.027$, we can compare the measured equilibrium height and velocity with the theoretical prediction as shown in Figs. 10a and 10b. Figure 10a shows the values of the equilibrium height (solid diamonds) as well as the interface thickness (vertical bars) used to calculate the values of the eddy efficiency parameter (Fig. 9). The least squares fit of the data that passes through the origin (dashed lines) shows good agreement between the experimental and predicted equilibrium height (Fig. 10a) and mean horizontal velocity (Fig. 10b).

In order to verify the geostrophic equilibrium hypothesis, we evaluated the geostrophic velocity between two density profiles as a function of the vertical depth assuming the free surface as a level of no motion. From these vertical profiles of velocity calculated along the radial section, we obtained an average geostrophic velocity at equilibrium for each experiment. The averaging was conducted using only the geostrophic velocities within the constant density bottom layer, that is, for the points below the open circles in Fig. 7a. The resulting averaged geostrophic velocities (not shown) presented more scatter, when compared to the predicted velocity Eq. (9), than the velocities measured by the potassium permanganate streaks.

We calculated the equilibrium transport T across the radial section for each experiment, using the profiles of geostrophic velocity. No dependence of the transport on g' and f was evident, in agreement with Eq. (10). Figure 11 shows that the measured transport is approximately 70% of the value predicted by Eq. (10). The scatter in Fig. 11 may be due to the similar scatter found in the averaged geostrophic velocities when compared with

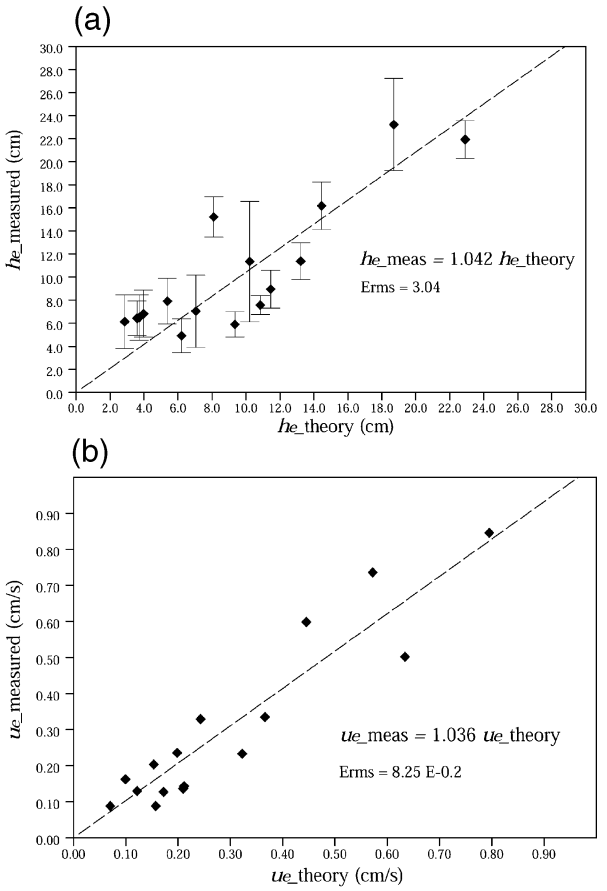

FIG. 10. Measured values of the (a) equilibrium height and (b) horizontal velocity compared with the predicted values obtained using Eqs. (8) and (9), respectively, and a value $c = 0.027$ for the eddy efficiency parameter.

[3] Prior studies of convective regions (Visbeck et al. 1996, 1997; Whitehead et al. 1996; Chapman and Gawarkiewicz 1997; Jones and Marshall 1997; Chapman 1998; Karsten et al. 2002; Marshall et al. 2002) employed similar scaling arguments and found values of c varying between 0.01 and 0.06. Spall and Chapman (1998) attempted to determine c theoretically by using a ''heton'' model of the lateral dispersion process and found a value of 0.045.

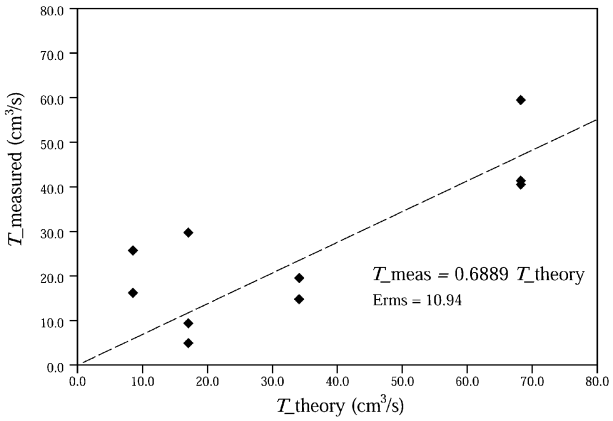

FIG. 11. Estimated values of the zonal transport across a radial section at equilibrium compared to the predicted values obtained using Eq. (10).

Eq. (9). The dependence on L could not be tested since L was a fixed parameter in our experiments.

5. Comparison with observations

The laboratory experiment described here is clearly a highly idealized representation of the ACC. Nevertheless it was designed to set up the essential dynamical balances that we believe pertain to the ACC, namely that the deepening of the thermocline in the ACC due to Ekman pumping is arrested by its baroclinic instability (Karsten et al. 2002; Marshall and Radko 2003). In order to predict the ACC thermocline depth based on the laboratory experiments, we first identify key nondimensional numbers that govern the experiments, and then ascertain the parameter regime of the ACC. Last, we evaluate the ACC thermocline depth using the laboratory scaling, given by Eq. (8).

a. Key nondimensional parameters

There are two key nondimensional parameters that measure the strength of buoyancy and mechanical forcing in our experiments. They are

1) a nondimensional deformation radius

$$\mathrm{Bu} = (R_c/L)^2 = (g'h_e)/(fL)^2,$$

which is a Burger number that compares the rotation time scale f^{-1} with the time it takes a gravity wave of speed $c_g = (g'h_e)^{1/2}$ to travel the width of the current L and

2) a mechanical forcing parameter

$$\mathrm{Ro} = w_e/h_e f,$$

which is a Rossby number that compares the rotation time scale with the vertical advective time scale h_e/w_e.

Our experiments fall in the nondimensional parameter space given by $1.7 \times 10^{-3} < \mathrm{Bu} < 6.5 \times 10^{-2}$ and $2.3 \times 10^{-5} < \mathrm{Ro} < 6.1 \times 10^{-4}$. The corresponding nondimensional parameter range for the ocean is

$$\mathrm{Bu} = \frac{g'h_e}{(fL)^2} = \frac{5 \times 10^{-3}10^3}{(10^{-4}2 \times 10^6)^2} \lesssim 10^{-4};$$

$$\mathrm{Ro} = \frac{w_e}{h_e f} = \frac{10^{-6}}{10^3 10^{-4}} \lesssim 10^{-5}.$$

We see that oceanic values are considerably smaller than those that can be achieved in our laboratory setup. However, Bu and Ro are small both in the laboratory and in the ocean. Reaching smaller values of Bu and Ro in the laboratory is infeasible since it would require either smaller g' (which would induce higher mixing between the dense and fresh water), or smaller w_e (which would increase the duration of the experiments making it comparable to diffusion time scales), or higher values of f (not possible or safe with the present experimental apparatus).

b. Estimates of ACC thermocline depth

To the extent that we can associate the height of the interface of our two-layer system with the depth of the thermocline in the circumpolar current, let us estimate the thermocline depth as predicted by Eq. (8). Inserting numbers typical of the Antarctic Circumpolar Current, $f = 1.2 \times 10^{-4}\ s^{-1}$, $w_e = 1.4 \times 10^{-6}$ m s^{-1} (corresponding to 50 m yr^{-1}), $g' = 5 \times 10^{-3}$ m s^{-2}, and $L = 2 \times 10^6$ m, then Eq. (8) predicts a maximum depth $h_e = 2200$ m. This is broadly consistent with (although somewhat larger than) the vertical e-folding scales of the buoyancy distribution found in gridded hydrographic observations of the ACC analyzed in Karsten and Marshall (2002). These e-folding scales range from a few hundred meters to 1500 m moving equatorward across the circumpolar flow from 63° to 43°S.

Our estimate is clearly sensitive to the numerical values assigned to the parameters in Eq. (8). However, it is significant, we feel, that Eq. (8) yields estimates that are directly in the observed range. Furthermore, if we use a more conservative estimate of the boundaries of the ACC, $L = 10^6$ m, we predict a maximum depth $h_e = 1320$ m, again consistent with the observed range given by Karsten and Marshall (2002). We conclude that the observed stratification in the ACC is consistent with the notion that it is set by the essential balance between Ekman pumping and lateral eddy transfer studied in our laboratory experiments and sketched schematically in Fig. 1.

Along with the depth scale we can evaluate the mean velocity scale u_e and the transport T for the ACC using Eqs. (9) and (10), respectively. For the numbers chosen above, we obtain $u_e = 4.6$ cm s^{-1} and $T = 200$ Sv (1 Sv $\equiv 10^6$ m^3 s^{-1}). These values are in the observed range for the ACC, where the average zonal current is approximately 5 cm s^{-1} and the zonal transport is ap-

proximately 130 ± 20 Sv, a value close to 70% (see section 4) of the predicted transport, $0.70T = 140$ Sv.

6. Conclusions

Inspired by our interest in the Antarctic Circumpolar Current, laboratory experiments were performed to investigate the influence of mechanical and buoyancy forcing in setting up the equilibrium stratification of a circumpolar front. In the small Ekman number limit, two nondimensional parameters characterize the flow: a scaled deformation radius, $\mathrm{Bu} = (R_c/L)^2$, which is a measure of the strength of the buoyancy forcing, and $\mathrm{Ro} = w_e/hf$, which is a measure of the strength of the mechanical forcing. The laboratory experiments spanned several orders of magnitude of these key parameters, enabling us to study the effects of a combination of mechanical and buoyancy forcing.

In our experiments the action of Ekman layers was represented by withdrawing ambient fluid from the middle of the tank (Fig. 2) and adding dense fluid in an annular region around the periphery. The dense fluid was continuously supplied creating a frontal region along which a current flowed in thermal wind balance. The current increased in height until it became baroclinically unstable and formed eddies that carried the dense fluid laterally away at a rate which balanced the supply of dense fluid from below. Thus the height of the current reached an equilibrium value, h_e, at which the rate of creation of potential energy, by combined mechanical and buoyancy forcing, balanced the rate at which it was released by baroclinic instability, as in the laboratory study of Marshall et al. (2002), numerical experiments of Karsten et al. (2002), and theory presented in Marshall and Radko (2003).

By applying an eddy flux closure inspired by Green (1970), which assumes that the eddy transfer scale is set by the width of the baroclinic current, we are able to relate the height and velocity of the equilibrated current to the external parameters f, w_e, and g' and an eddy efficiency parameter c [see Eqs. (8) and (9)]. Note that our observed equilibrium heights and velocities are not consistent with a scaling based on the assumption that the eddy transfer scale is set by the deformation scale, $\sqrt{g'h_e}/f$, rather than L, the scale of the current. The former assumption is made, for example, in Stone (1972) and Griffiths and Hopfinger (1984). The latter is assumed in Green (1970), Jones and Marshall (1997), and Marshall et al. (2002). The distinction matters in this experiment because $\mathrm{Bu} \ll 1$. As described in section 4, we determined c by assuming that the radial volume flux, required at equilibrium to balance sources and sinks, is achieved by eddies. The values obtained for c ranged between 0.01 and 0.06 with a scatter of the same magnitude as in the previous studies mentioned in the footnote in section 4a. Using the average value of $c = 0.027$, measured and predicted equilibrium heights and horizontal velocity scales (Fig. 10) compared remarkably well. The particular parameter dependencies suggested by Eqs. (8) and (9)—for example, that the depth of the ACC depends on $\sqrt{\tau}$ and the transport on τ (where τ is the wind stress)—are a consequence of the eddy flux closure assumed [see, in particular, Eq. (6)]. The agreement between the experimental results and the scaling predictions lends strong support to this eddy flux closure.

Our study is in support of the arguments presented in Karsten et al. (2002) and Marshall and Radko (2003) that the stratification and depth of the ACC are set by its baroclinic instability. When applied to the ACC, we obtain depth and velocity scales (see section 5) plausibly close to observed values.

Acknowledgments. We thank the Physical Oceanography Division of the National Science Foundation whose support made this study possible under Grant OCE-0095427. The laboratory experiments could not have been carried out without the assistance of Keith Bradley, whom we thank.

REFERENCES

Beardsley, R. C., 1969: A laboratory model of the wind-driven ocean circulation. *J. Fluid Mech.,* **38,** 255–271.

——, 1973: A numerical model of the wind-driven ocean circulation in a circular basin. *Geophys. Fluid Dyn.,* **4,** 211–241.

——, 1975: The 'sliced-cylinder' laboratory model of the wind-driven ocean circulation. Part 2: Oscillatory forcing and Rossby wave resonance. *J. Fluid Mech.,* **69,** 41–64.

——, and K. Robbins, 1975: The 'sliced-cylinder' laboratory model of the wind-driven ocean circulation. Part 1: Steady forcing and topographic Rossby wave instability. *J. Fluid Mech.,* **69,** 27–40.

Becker, A., and M. A. Page, 1990: Flow separation and unsteadiness in a rotating sliced cylinder. *Geophys. Astrophys. Fluid Dyn.,* **55,** 89–115.

Cenedese, C., and P. F. Linden, 2002: The stability of a buoyancy-driven coastal current at the shelfbreak. *J. Fluid Mech.,* **452,** 97–121.

Chapman, D. C., 1998: Setting the scales of the ocean response to isolated convection. *J. Phys. Oceanogr.,* **28,** 606–620.

——, and G. Gawarkiewicz, 1997: Shallow convection and buoyancy equilibration in an idealized coastal polynya. *J. Phys. Oceanogr.,* **27,** 555–566.

Chia, F. R., R. W. Griffiths, and P. F. Linden, 1982: Laboratory experiments on fronts. Part II. The formation of cyclonic eddies at upwelling fronts. *Geophys. Astrophys. Fluid Dyn.,* **19,** 189–206.

Condie, S., and P. B. Rhines, 1994: A convective model for the zonal jets in the atmosphere of Jupiter and Saturn. *Nature,* **367,** 711–713.

Douglas, R. A., R. Hide, and P. J. Mason, 1972: An investigation of the structure of baroclinic waves using three-level photography. *Quart. J. Roy. Meteor. Soc.,* **98,** 247–263.

Eady, E. T., 1949: Long waves and cyclone waves. *Tellus,* **1,** 35–52.

Green, J. S., 1970: Transfer properties of the large-scale eddies and the general circulation of the atmosphere. *Quart. J. Roy. Meteor. Soc.,* **96,** 157–185.

Griffiths, R. W., and P. F. Linden, 1981a: The stability of vortices in a rotating, stratified fluid. *J. Fluid Mech.,* **105,** 283–316.

——, and ——, 1981b: The stability of buoyancy-driven coastal currents. *Dyn. Atmos. Oceans,* **5,** 281–306.

——, and ——, 1982: Laboratory experiments on fronts. Part I. Density driven boundary currents. *Geophys. Astrophys. Fluid Dyn.,* **19,** 159–187.

——, and E. F. Hopfinger, 1984: The structure of mesoscale turbulence and horizontal spreading at ocean fronts. *Deep-Sea Res.*, **33,** 245–269.
——, and G. Veronis, 1997: A laboratory study of the effects of a sloping side boundary on wind-driven circulation in a homogeneous ocean model. *J. Mar. Res.*, **55,** 1103–1126.
——, and ——, 1998: Linear theory of the effect of a sloping boundary on circulation in a homogeneous laboratory model. *J. Mar. Res.*, **56,** 75–86.
Hart, J. E., 1972: A laboratory study of baroclinic instability. *Geophys. Fluid Dyn.*, **3,** 181–209.
——, 1980: An experimental study of nonlinear baroclinic instability and mode selection in a large basin. *Dyn. Atmos. Oceans,* **4,** 115–135.
Hide, R., 1971: Laboratory experiments of free thermal convection in a rotating fluid subject to a horizontal temperature gradient and their relation to the theory of the global atmospheric circulation. *The Global Circulation of the Atmosphere,* G. A. Corby, Ed., Royal Meteorological Society, 196–221.
Ivey, G. N., J. R. Taylor, and M. J. Coates, 1995: Convectively driven mixed layer growth in a rotating, stratified fluid. *Deep-Sea Res.*, **42,** 331–349.
Jones, H., and J. Marshall, 1997: Restratification after deep convection. *J. Phys. Oceanogr.*, **27,** 2276–2287.
Karsten, R., and J. Marshall, 2002: Testing theories of the vertical stratification of the ACC against observations. *Dyn. Atmos. Oceans,* **36,** 233–246.
——, H. Jones, and J. Marshall, 2002: The role of eddy transfer in setting the stratification and transport of a circumpolar current. *J. Phys. Oceanogr.*, **32,** 39–54.
Marshall, J., and T. Radko, 2003: Residual-mean solutions for the Antarctic Circumpolar Current and its associated overturning circulation. *J. Phys. Oceanogr.*, **33,** 2341–2354.
——, H. Jones, R. Karsten, and R. Wardle, 2002: Can eddies set ocean stratification? *J. Phys. Oceanogr.*, **32,** 26–32.
Narimousa, S., and T. Maxworthy, 1985: Two-layer model of shear-driven coastal upwelling in the presence of bottom topography. *J. Fluid Mech.,* **159,** 503–531.
——, and ——, 1987: Coastal upwelling on a sloping bottom: The formation of plumes, jets and pinched-off cyclones. *J. Fluid Mech.,* **176,** 169–190.
Pedlosky, J., and H. P. Greenspan, 1967: A simple laboratory model for the oceanic circulation. *J. Fluid Mech.,* **27,** 291–304.
Phillips, N. A., 1954: Energy transformations and meridional circulations associated with simple baroclinic waves in a two-level, quasi-geostrophic model. *Tellus,* **6,** 273–286.
Radko, T., and J. Marshall, 2003: Equilibration of a warmed, pumped lens on a beta plane. *J. Phys. Oceanogr.*, **33,** 885–899.
Rhines, P., 1994: Jets. *Chaos*, **4,** 313–339.
Rosman, J. H., P. Jacobs, and G. N. Ivey, 1999: The effects of a surface stress-driven ambient circulation on open ocean convection. *Geophys. Astrophys. Fluid Dyn.*, **91,** 199–222.
Saunders, P. M., 1973: The instability of a baroclinic vortex. *J. Phys. Oceanogr.,* **3,** 61–65.
Sommeria, J., S. D. Meyers, and H. L. Swinney, 1989: Laboratory model of a planetary eastward jet. *Nature,* **337,** 58–61.
——, ——, and ——, 1991: Experiments on vortices and Rossby waves in eastward and westward jets. *Nonlinear Topics in Ocean Physics: Proceedings of the Enrico Fermi Summer School,* A. Osborne, Ed., Elsevier Science, 227–269.
Spall, M. A., and D. C. Chapman, 1998: On efficiency of baroclinic eddy heat transport across narrow fronts. *J. Phys. Oceanogr.*, **28,** 2275–2287.
Stone, P., 1972: A simplified radiative–dynamical model for the static stability of rotating atmospheres. *J. Atmos. Sci.,* **29,** 405–418.
Visbeck, M., J. Marshall, and H. Jones, 1996: Dynamics of isolated convective regions in the ocean. *J. Phys. Oceanogr.,* **26,** 1721–1734.
——, ——, T. Haine, and M. Spall, 1997: On the specification of eddy transfer coefficients in coarse-resolution ocean circulation models. *J. Phys. Oceanogr.,* **27,** 381–402.
Whitehead, J. A., J. Marshall, and G. E. Hufford, 1996: Localized convection in rotating stratified fluid. *J. Geophys. Res.,* **101,** 25 705–25 721.